NJC

Accepted Manuscript

This is an *Accepted Manuscript*, which has been through the Royal Society of Chemistry peer review process and has been accepted for publication.

Accepted Manuscripts are published online shortly after acceptance, before technical editing, formatting and proof reading. Using this free service, authors can make their results available to the community, in citable form, before we publish the edited article. We will replace this *Accepted Manuscript* with the edited and formatted *Advance Article* as soon as it is available.

You can find more information about *Accepted Manuscripts* in the Information for Authors.

Please note that technical editing may introduce minor changes to the text and/or graphics, which may alter content. The journal's standard Terms & Conditions and the Ethical guidelines still apply. In no event shall the Royal Society of Chemistry be held responsible for any errors or omissions in this *Accepted Manuscript* or any consequences arising from the use of any information it contains.

ROYAL SOCIETY OF CHEMISTRY

www.rsc.org/njc

NJC

ARTICLE

In vitro investigation of the interaction between the hepatitis C virus drug sofosbuvir and human serum albumin through ^{1}H NMR, molecular docking, and spectroscopic analysis

Received 00th January 20xx,
Accepted 00th January 20xx

DOI: 10.1039/x0xx00000x

www.rsc.org/

Hongqin Yang[a], Yanmei Huang,[a] Di Wu[a], Jin Yan[a], Jiawei He[a], Hui Li*[a]

Sofosbuvir (SOF), an oral nucleotide inhibitor of the nonstructural protein 5B RNA of the hepatitis C virus (HCV), was approved for treating chronic HCV infection by the Food and Drug Administration in 2013. Understanding drug–protein interactions is a crucial factor in determining the pharmacokinetics and pharmacodynamics of a drug. In this study, the interaction between SOF and human serum albumin (HSA) was investigated using ^{1}H nuclear magnetic resonance (NMR) spectroscopy, the molecular docking method, fluorescence, Fourier transform infrared (FT-IR) and circular dichroism (CD) spectroscopy. The analysis of saturation transfer difference (STD) and WaterLOGSY data indicated that SOF was bound to HSA, and the STD signals showed that the methyl and aromatic protons of the hydrophobic components of SOF have the most intimate contact with protein. The negative free energies (−7.17 kcal mol^{-1} and −6.18 kcal mol^{-1}) obtained from molecular docking and fluorescence studies clearly suggested the spontaneity of the interaction of the SOF–HSA complex. STD, WaterLOGSY and fluorescence displacement experiments demonstrated that SOF was preferentially bound to site I of HSA, and this finding was supported by the docking results. In addition, synchronous and three-dimensional (3D) fluorescence, FT-IR, and CD spectrocopy provided complementary informations on the micro-environmental and conformational changes of HSA with the addition of SOF. The combination of ^{1}H NMR and conventional methods provided useful information to elucidate further the binding mechanisms of antiviral drugs with HSA.

1. Introduction

Chronic hepatitis C (CHC), a serious disease caused by hepatitis C virus (HCV) infection, is a serious threaten to human health, with approximately 200 million individuals infected worldwide.[1] The co-infection of HCV with the human immunodeficiency virus (HIV) and other human pathogens has resulted in high morbidity and mortality rates and has increased the risk of liver cirrhosis and hepatocellular carcinoma.[2-6] To address this global challenge, health authorities have required the development of innovative therapeutic strategies to combat HCV infection. The current standard treatment regimen for HCV-infected patients is a combination of regular injections of pegylated interferon (IFN) and oral ribavirin (RBV) therapy.[7] However, the low sustained virological response (SVR) rate, dosing, drug interaction, and side effects restrict the use of IFN and RBV combined therapy.[3, 8] In 2013, the Food and Drug Administration (FDA) approved the use of sofosbuvir (SOF, Fig. 1) (Sovaldi; Gilead Sciences, Foster City, CA, USA), a new oral nucleotide inhibitor that exhibits satisfactory activity against the HCV nonstructural protein 5B (NS5B) RNA,[9-12] for treating HCV patients with HIV-1 co-infection.[13] SOF is a prodrug of 2'-deoxy-2'-fluoro-2'-C-methyluridine monophosphate that is converted to its active uridine triphosphate form within the hepatocytes, which terminates the RNA chain.[9] SOF-based treatments have demonstrated SVR rates of over 90% across genotypes; hence, this drug offers new prospects to HCV-infected patients.[14]

After its oral administration, SOF enters the bloodstream and binds to plasma proteins and lipids or becomes freely available.[7] Plasma protein binding (PPB) is considered as an important parameter throughout an ongoing drug development program.[15] Many factors, such as drug absorption, distribution, free concentration, and metabolism, are affected by drug–protein interactions in the bloodstream.[16-19] A considerable number of prodrugs combine with plasma protein to protect their pharmacophore, which helps prodrugs reach their target cells, and consequently, results in healing efficacy. Given the high concentration of albumin in human blood plasma and its high binding affinity to a wide range of drugs, human serum albumin (HSA) has been the most extensively used model protein to evaluate drug–protein systems.[15, 20, 21] The primary structure of HSA is well-known and its crystal structure has also been measured by X-ray crystallography, which indicates that HSA is a monomeric protein that contains 585 amino acids with 3 homologous α-helical domains (I–III), each with subdomains A and B.[19, 22] Sudlow I and Sudlow II

[a] College of Chemical Engineering. Sichuan University, Chengdu 610065, China; Tel.: +86 028 85405149; Fax: +86 028 85401207.
E-mail: lihuilab@sina.com (Hui, Li)

are the two primary drug-binding sites in HSA that are located in the hydrophobic subdomains IIA and IIIA, which are called sites I and II, respectively.[23, 24] Studies on the interactions between drugs and HSA have received increasing attention in therapeutic drug monitoring; they have significantly contributed to the understanding of the pharmacological behavior and several biological and physicochemical mechanisms of drugs transported in the human body.[18, 19, 25, 26]

Several studies have demonstrated the interaction between antiviral drugs and biological macromolecules through spectroscopy and X-ray crystallography,[26, 27] as well as non-spectroscopic research such as ProteinChip serum analysis.[8] Although numerous articles in literature have discussed the safety and clinical efficacy of these antiviral drugs,[1, 7-9, 28] their protein-binding mechanisms have not been fully elucidated. Several methods have been utilized to explain the interaction mechanisms between drugs and proteins, such as isothermal titration calorimetry,[22, 29] equilibrium dialysis,[30] electrophoretic techniques,[31, 32] and spectroscopic analysis.[33, 34] Another technique used to study drug-protein systems is nuclear magnetic resonance (NMR), which is a powerful tool for probing and understanding weak binding processes at the molecular level. Accordingly, a saturation transfer difference (STD) and WaterLOGSY experiment is appropriate because it can identify the small molecules involved in structural information without protein labelling. In the present work, a qualitative study of the interaction between SOF and HSA was conducted using ^{1}H NMR methodology, molecular dynamic simulation was performed to visualize binding properties. Moreover, we used fluorescence spectroscopy to determine binding information, including quenching mechanisms, binding constants, and thermodynamic parameters. The effects of SOF on the microenvironment of tryptophan (Trp) residue as well as on the conformation of HSA were also interpreted based on synchronous fluorescence, 3D fluorescence, FT-IR spectra and CD spectra.

2. Materials and Methods

2.1 Materials

HSA free from essential fatty acids was purchased from Sigma-Aldrich (Milwaukee, USA) and used without further purification. SOF was purchased from Aladdin Chemical Reagent (Shanghai, China). Warfarin, ibuprofen, Na_2HPO_4, and NaH_2PO_4 were supplied by DaLian MeiLun Biology Technology Co., Ltd. (DaLian, China). Deuterium oxide (D_2O, 99.9% purity) and dimethyl sulfoxide-d6 (DMSO-d6) were purchased from the J&K Scientific Ltd. (Beijing, China). Triple-distilled water was used to prepare the phosphate buffer solution (PBS) and stock solutions of SOF (2×10^{-3} M). The stock solutions of HSA (2.0×10^{-5} M) were prepared by dissolving solid HSA into 0.05 M PBS at pH 7.4 and stored at 0–4 ℃ in a dark environment. Warfarin (2×10^{-3} M) and ibuprofen (2×10^{-3} M) were prepared in anhydrous ethanol. All other reagents were of analytical grade and used as purchased without further purification.

2.2 NMR technique

All NMR experiments were acquired on a Varian 700 MHz Inova spectrometer operating at 298K, running under VNMRJ software (version 2.1B). The stock solution of SOF (4×10^{-2}M), warfarin (8×10^{-2} M) and ibuprofen (8×10^{-2} M) were prepared in DMSO-d6 and diluted by 0.05 M PBS [50% (v/v)D2O and H2O mixture] for further use. NMR samples were prepared in 500 μL 0.01 M PBS buffer [50% (v/v) D_2O and H_2O mixture], with pH 7.4 at room temperature, to final concentrations of 1×10^{-5} M HSA and 4×10^{-4} M SOF (molar ratio of HSA to SOF = 1:40). Competition studies were performed with warfarin and ibuprofen, two known binders of site I and site II of HSA, respectively. Samples included identical HSA and SOF concentration and Warfarin (8×10^{-4} M) or ibuprofen (8×10^{-4} M) were analysed. For STD measurement, a number of 50 ms Gaussian pulses were applied, and these pulses were applied at on-resonance saturation of -0.5 ppm and off-resonance saturation of 34 ppm. All the spectra were acquired by using sweep width of 8389.26 Hz, number of transients 256 and acquisition time of 1 s. The total number of scans was 1024, and typically using 16 ppm spectral widths for the ^{1}H STD spectra. The subtraction was performed after every STD scan by phase cycling. WaterLOGSY spectra were acquired in 256 transients, 32768 complex data points, 9842.52 Hz sweep width and 0.999947 s acquisition time. Each sample was recorded with Watergate solvent suppression to obtain a standard ^{1}H spectrum. All spectra were processed and analyzed using ACD/CNMR software (Advanced Chemistry Development, Inc., version 11.0)

2.3 Molecular docking

MGLTools 1.5.6 AutoDockTools (ADTs) with AutoGrid 4 and AutoDock 4 were used to set up and conduct docking calculations between SOF and HSA. The crystal structure of free HSA was obtained from the Research Collaboratory for Structural Bioinformatics Protein Data Bank (PDB ID: 1H9Z; http://www.pdb.org) and all water molecules were removed. Polar hydrogen atoms were then added and calculation of Gasteiger charges followed. The three-dimensional (3D) structure of SOF was generated using Chem3D Ultra 11.0 and energy was minimized using the "Discover Minimization" tool in Materials Studio 6.0. The PDB partial charge and atom type (PDBQT) files of the receptor (HSA) and drug (SOF) were prepared using ADTs, and the pH of the receptor was adjusted to nearly neutral (7.4). For drug preparation, 12 rotatable bonds were defined in the multi-conformation docking given that SOF structure was flexible. Lamarckian genetic algorithms (LGA) were employed to simulate the interaction between the receptor and the drug and to describe their relationship through the translation, orientation, and conformation of the drug in AutoDock. To recognize the binding site of SOF in HSA, the blind docking simulation strategy was adopted by setting grid box size to 126 Å × 126 Å × 126 Å along the X, Y, and Z axes, respectively, with 0.619 Å grid spacing. The center of the grid was set to the position of 23.758, 7.805, and 16.725. Global optimization started with 200 runs in a moderate number of 250,000 energy evaluations and a maximum of 27,000 generations. Other parameters were set as the default protocol settings. Subsequently, the lowest energy docked conformation was applied to locate the most suitable binding mode further.

2.4 Fluorescence spectroscopy

Fluorescence measurements were performed using a Cary Eclipse fluorescence spectrophotometer (Varian, USA) equipped with a 1.0 cm quartz cell. HSA concentration was diluted to 2.0×10−6 M with PBS buffer solution. The final drug concentrations (0.0–5.3×10−5 M) were obtained by titrating 2.0×10−3 M SOF stock solutions in each 5 mL volumetric flask. Experiments were performed at three temperatures (298, 304, and 310 K) in a thermostat water bath for 1 h before fluorescence measurements. The emission wavelength was read at 290–500 nm with an excitation wavelength at 280 nm, i.e., excitation of Trp and tyrosine (Tyr), and the emission and excitation slit widths were fixed at 5 nm and 10 nm, respectively.

Competitive site-marker fluorescence experiments were performed at 298 K to determine the specific binding sites of SOF in HSA in an HSA–SOF solution at a molar ratio of 1:5. The concentrations of probes ranging from 2.0×10−6 M to 2.0×10−5 M in the solution were obtained by gradually adding an increment (2.0×10−6 M) of probe stock solution into the HSA–SOF solution. Their fluorescence intensities were recorded under the same experimental conditions described earlier.

The synchronous fluorescence spectra of HSA with various SOF concentrations were recorded at 298 K by considering wavelength intervals $\Delta\lambda$ = 15 nm and 60 nm to determine Tyr and Trp residues, respectively ($\Delta\lambda = \lambda_{em} - \lambda_{ex}$). 3D fluorescence spectra of HSA (2.0×10^{-6} M) and HSA–SOF solutions (molar ratio, 1:10) were scanned under the following conditions: the emission wavelength was recorded between 200 and 500 nm; the initial excitation wavelength was 200 nm with increments of 5 nm; other scanning parameters were identical to the above of the fluorescence emission spectra.

2.5 FT-IR spectroscopy

The IR spectra of HSA in presence and absence of SOF were recorded in the range of 4000–600 cm^{-1} on a Nicolet-6700 FTIR spectrometer (Thermo, USA) with a smart OMNI-sampler accessory. The spectra were obtained by the attenuated total reflection method with resolution of 4 cm^{-1} and 64 scans at 298K. HSA concentration was fixed at 2×10^{-4} M while that of SOF was 1 mM.

2.6 CD spectroscopy

CD spectra measurements were conducted using an automatic recording spectrophotometer (Model 400, AVIV, USA) in a 2 mm path length cell at 298 K. Each spectrum was the average of three successive scans within the wavelength range of 200–250 nm. The experiments were performed by keeping HSA concentration constant (3.0×10^{-6} M) while varying SOF concentration at 0–4.5×10^{-5} M (i.e., [SOF]/[HSA] = 0, 5, and 15).

3. Results and discussion

3.1 NMR spectroscopy studies

The NMR technique is extensively used in various engineering problems, particularly for screening applications in the pharmaceutical industry to detect the binding of small molecular compounds to biological macromolecules.[35-37] In recent years, STD and WaterLOGSY NMR experiments have been applied to characterize drug–protein interaction as a new NMR-based screening method.[36, 38-40] Both STD and WaterLOGSY are based on intermolecular NOEs to the transiently bound ligand ^{1}H. For the STD method, its high sensitivity provides the most intense NMR signals for the small molecular compound that exhibits the strongest contact to a protein without any labelling and separation requirements. Previous studies found that STD–NMR spectra only contained the signals of each ligand proton bound to a protein.[35, 36] In the case of WaterLOGSY method, its standard application is in primary screening of weak ligands with dissociation contants in the μM to mM range.[41]

In the present study, the reference ^{1}H NMR spectrum of the SOF–HSA system and the corresponding STD–NMR spectrum obtained in the experiment were displayed in Figs. 1(a) and 1(b), respectively. As shown in Fig. 1, protein saturation spread onto the drug (SOF) because of similar characteristic signals between the ^{1}H NMR and STD–NMR spectra. Obvious STD effects were observed for the H-8, 9, CH_3-13, 20, 27, 28, and the aromatic protons of the SOF molecule, which indicated that the SOF bound to HSA. As a complementary technique, WaterLOGSY experiments were further performed [Supplementary file: Fig. S1(a)]. The positive signals of spectrum (a) corresponding to the methyl groups and the aromatic protons in Fig. S1(a) is believed to be due to the weak interaction between SOF and HSA. All these findings showed that SOF was inserted into the hydrophobic cavities of HSA and the hydrophobic components of the drug were the most tightly bound to HSA. Consequently, the ^{1}H STD–NMR technique can effectively detect and characterize the bonding information of SOF–HSA. Drug–protein interactions play a key role in the cardiovascular system. In particular, a prodrug can be temporarily stored in the plasma by forming a protein complex to prolong action time and decrease adverse reactions.

To identify which of the plentiful binding site of HSA the SOF was interacting with, competitive STD–NMR experiments were carried out in the presence of warfarin and ibuprofen, two the reference site-markers to sites I and II of HSA, respectively.[23] For this, the site-marker was added to a solution containing fixed amounts of ligand and HSA system could reflect a direct competition at the corresponding of site. The competitive STD–NMR spectra for SOF–HSA system were presented in Fig. 2. As shown in Figs. 2 (a), (b) and (c), with the addition of a site-marker into SOF-HSA solution, the STD signals were lower than that of without a site-marker. Although competition of the ligands from both sites I and II of HSA, according to the STD signal intensities, a larger decrease occurred in the presence of warfarin for the protons of bound ligand, which indicated that binding to site I was favoured over site II. Furthermore, to facilitate the comparison of the influence of warfarin and ibuprofen on the binding of SOF to HSA, the WaterLOGSY experiments in the presence of the two site-markers were carried out [Supplementary file: Fig. S1 (b) and (c)]. The waterLOGSY responsing to addition of site-marker showed clear negative signals when titrated with warfarin rather than ibuprofen, which confirmed the STD finding, namely the binding site of SOF was located preferentially within site I of HSA.

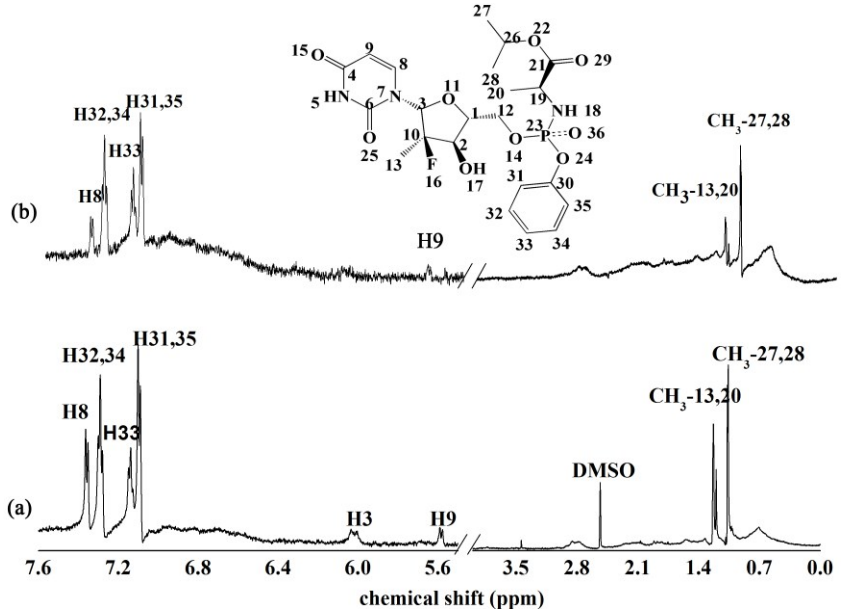

Fig. 1 ^{1}H NMR spectrum of SOF and HSA in 40:1 ratio recorded with a Watergate scheme for solvent suppression (a) and the corresponding STD spectrum (b).

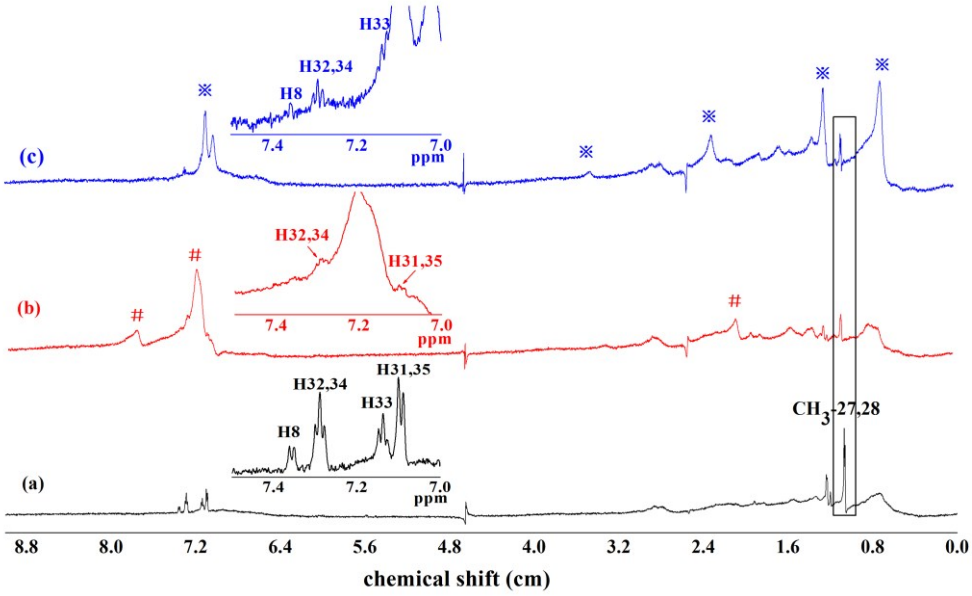

Fig. 2 STD spectra of (a) a solution containing 4×10^{-4} M SOF and 1×10^{-5} M HSA, (b) 8×10^{-4} M warfarin was added to (a) solution, (c) 8×10^{-4} M ibuprofen was added to (a) solution**.** The signals of competitor are indicated by # (warfarin) and ※ (ibuprofen).

3.2 Analysis of molecular docking

To obtain comprehensive insight into the binding of SOF with HSA, the molecular docking method was used to determine the binding orientation of the SOF molecule onto HSA and to provide predictions on the outcome of fluorometric experiments. All solutions to the experiments may be close to the physiological conditions but the binding orientation of small molecules is difficult to determine at the atomic level. Molecular docking methods have been extensively used in drug-based structural screening techniques to screen out the preferred binding location between drugs and proteins, which can substantiate our experimental results.[33, 42-45] In our experiment, the binding site of the drug (i.e., SOF) in HSA was based on the docking simulation performed according to the AutoDock 1.5.6 program. From the docking calculation, eight multimember conformational clusters were collected and shown in Fig. 3. The highest populated cluster accounted for over half of the obtained conformations and observed to be the lowest on the binding energy range. With energy visualization, the overall docking energies for a drug molecule in its active site are expressed by the following equation:

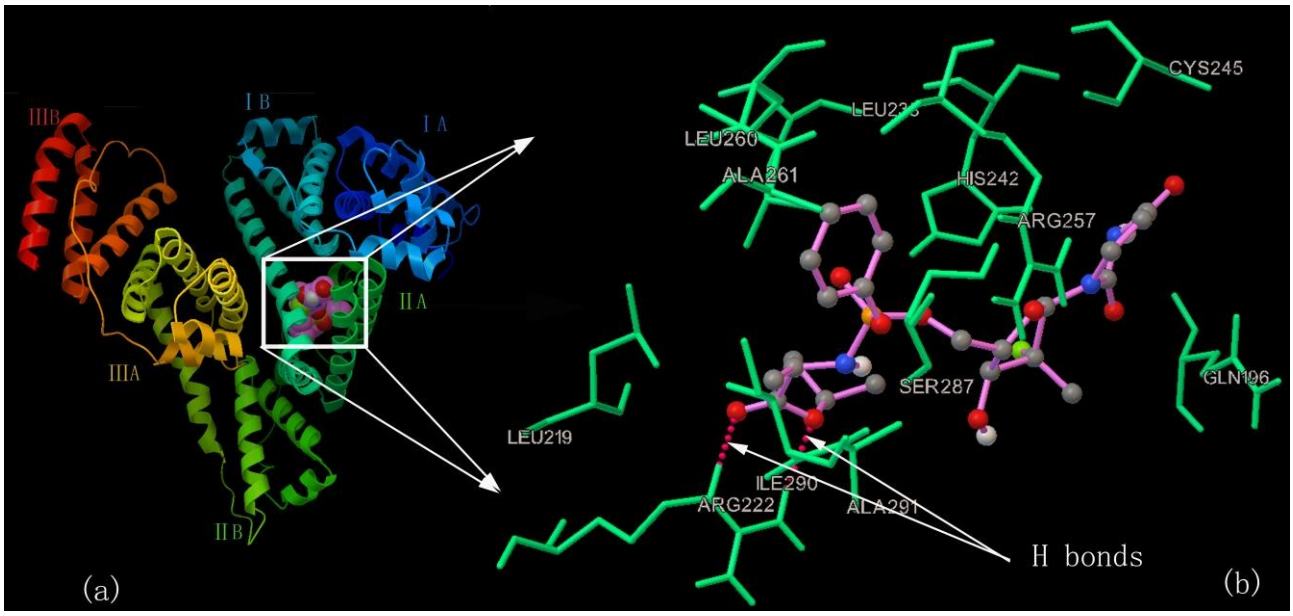

Fig. 4 Molecular docking analysis results. (a) Docking simulation shows that SOF is located within the hydrophobic cavity of IIA subdomain in HSA. (b) Amino acid residues that surround the bound SOF. The red dotted lines indicate the formation of the hydrogen bond.

$$\Delta G = \Delta G_{vdW} \sum_{ij}\left(\frac{A_{ij}}{r_{ij}^{12}} - \frac{B_{ij}}{r_{ij}^{6}}\right) + \Delta G_{hbond} \sum_{ij}\left(\frac{C_{ij}}{r_{ij}^{12}} - \frac{D_{ij}}{r_{ij}^{10}} + E_{hbond}\right) + \Delta G_{elec} \sum_{ij}\frac{q_i - q_j}{s(r_{ij})r_{ij}} + \Delta G_{tor} N_{tor} + \Delta G_{sol} \sum_{icj} S_i V_j e^{\left(-r_{ij}^2/2\sigma^2\right)} \quad (1)$$

where ΔGvdW, ΔGhbond, ΔGelec, ΔGtor, and ΔGsol are the free energy coefficients of the van der Waals force, hydrogen bond, electrostatic interactions, torsional interactions, and desolvation energy of the drug–HSA complex, respectively. rij is the interatomic distance, Aij and Bij represent the depths of energy well, Cij and Dij represent the equilibrium separations between the two atoms. The first three terms represent the vacuo force field energies for intermolecular interactions, while the fourth term denotes the internal steric energy of the drug molecule. The fifth term indicates the total desolvation energy of the drug–HSA complex. These energies can be computed and distinguished by the end result of docking. In this study, we presented the energies of the top 10 SOF conformers in this cluster (Table 1).

The optimal docked result shows that one SOF molecule occupies the center of the hydrophobic cavity of subdomain IIA in Sudlow site I of HSA (Fig. 4). The SOF molecule is surrounded by hydrophobic residues (Leu219, Arg222, Leu238, His242, Arg257, Leu260, Ala261, Ser287, and Ala291) and polar residues (Cys245 and Ile290), which confirms that the binding phenomenon is mainly governed by a hydrophobic force with few minimal electrostatic interactions. In addition, the molecular docking data show that two hydrogen bonds are present in the SOF–HSA system, namely, the 22-O and 29=O of SOF, which form two hydrogen bonds with residue Arg222. Furthermore, the formed hydrogen bonds have bond energies of −4.56 kcal mol−1 and −5.68 kcal mol−1 and bond distances of 2.16 Å and 1.65 Å, respectively. Based on the data, hydrophobic forces play a major role in binding SOF to HSA, while other forces, including electrostatic interactions and hydrogen bonds, are also present. The docking results corroborate the accuracy of the 1H NMR measurement, which coincides with the hydrophobic groups of SOF to participate directly in the interaction with protein.

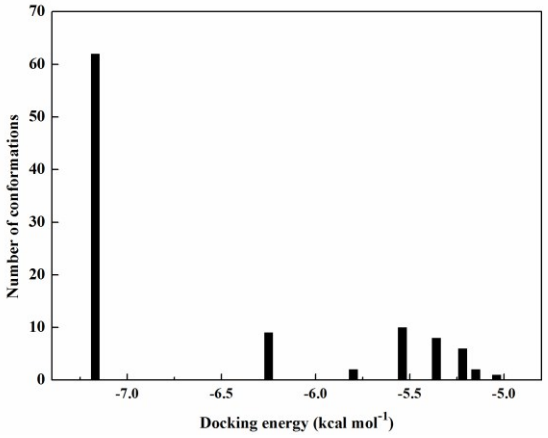

Fig. 3 Cluster analyses of the AutoDock docking runs of the SOF–HSA system.

Table 1 Summary of the docking results of SOF bound to HSA in the highest populated cluster according to the AutoDock program that generated different drug conformers (top 10).

Rank	ΔG (kcal/mol)	G_{vdW} (kcal/mol)	G_{hbond} (kcal/mol)	G_{elect} (kcal/mol)	G_{tor} (kcal/mol)	G_{total} (kcal/mol)	clRMS	refRMS
1	−7.17	−10.52	−10.75	−0.23	3.58	−1.72	0.00	33.94
2	−7.16	−10.52	−10.74	−0.22	3.58	−1.72	0.09	33.95
3	−7.15	−10.55	−10.73	−0.18	3.58	−1.66	0.70	34.08
4	−7.15	−10.54	−10.73	−0.19	3.58	−1.65	0.68	34.06
5	−7.15	−10.55	−10.73	−0.18	3.58	−1.67	0.69	34.07
6	−7.14	−10.49	−10.72	−0.23	3.58	−1.76	0.09	33.94
7	−7.14	−10.53	−10.72	−0.19	3.58	−1.61	0.64	34.09
8	−7.14	−10.54	−10.72	−0.18	3.58	−1.59	0.70	33.99
9	−7.14	−10.54	−10.72	−0.17	3.58	−1.58	0.64	34.01
10	−7.13	−10.54	−10.71	−0.17	3.58	−1.67	0.72	34.05

3.3 Fluorescence quenching spectral studies

The fluorescence of many proteins is caused by three intrinsic fluorophores, namely, Trp, Tyr, and phenyalanine residues, with the last contributing only slightly.[15, 19] Literature has established that the emission spectrum of HSA depends on the degree of exposure of Trp residues to solvent polarity.[46] Some small molecules can change the microenvironment of a fluorophore, which changes the intrinsic fluorescence intensity of HSA. In the present work, the measurements of HSA fluorescence excited at 280 nm were performed by adding SOF into proteins at 298, 304, and 310 K. The effect of SOF on the fluorescence intensity of HSA was displayed in Fig. 5, from which HSA is observed to have an obvious fluorescence emission band at 338 nm, which is gradually quenched by adding various amounts of SOF at 298 K. In addition, SOF alone does not emit fluorescence at the highest concentration (Fig. 5). Therefore, the observed decrease in fluorescence intensity can be ascribed to the binding of SOF with HSA, which is consistent with the results obtained in the ^{1}H NMR and molecular docking investigations

3.3.1 Quenching mechanism and binding constant

The quenching mechanism is frequently categorized into static quenching and dynamic quenching, which represent two entirely different quenching processes.47 Both quenching mechanisms can be distinguished by their differential dependence on temperature. A high temperature results in fast diffusion and strong collisional quenching; hence, a large extent of dynamic quenching with the quenching constant is increased. By contrast, the effect is typically reversed in static quenching, i.e., the quenching constant is reduced with increasing temperature because of the formation of a ground state complex with protein.22, 25, 33, 36 For a detailed evaluation of the quenching mechanism, the Stern–Volmer equation is used to analyze the decrease in fluorescence intensity, as follows48:

$$\frac{F_0}{F} = 1 + K_{sv}[Q] \quad (2)$$

where F_0 and F are the fluorescence intensities in the absence and presence of a quencher, respectively; [Q]is the concentration of the quencher; and K_{sv} represents the Stern–Volmer quenching constant, which is:

$$K_{sv} = K_q \tau_0 \quad (3)$$

where K_q is the quenching rate constant of the biological macromolecules, and τ_0 is the average lifetime of the biological macromolecules in the absence of a quencher; the value of τ_0 is 10^{-8} s for HSA.[18, 22] The plot of F_0/F versus [Q] is linear, with K_{sv} as the slope (Fig. 6). The values of K_{sv} and K_q for the SOF–HSA system at three different temperatures are given in Table 2. The results show that the values of K_{sv} decrease with increasing temperature, and the values of K_q are greater than the limiting diffusion rate constant of biological macromolecules (2×10^{10} L mol^{-1} s^{-1}).[49] Thus, the quenching of HSA by SOF is attributed to the formation of the ground state complex via the static quenching process.[18, 47]

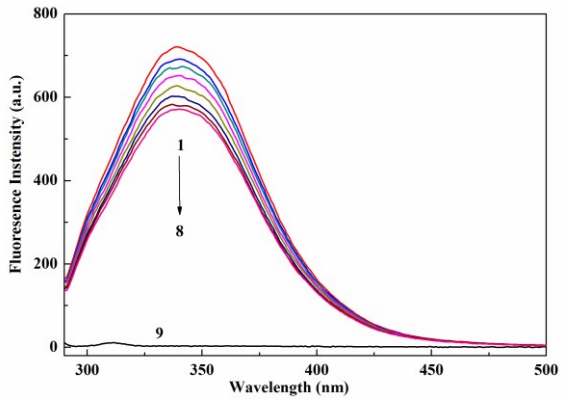

Fig. 5 Fluorescence emission spectra of HSA (2.0×10^{-6} M) at various SOF concentrations. Curves 1 → 9 correspond to C_{SOF} = 0, 0.5, 1.3, 2.1, 2.3, 3.7, 4.5, 5.3×10^{-5}, 5.3×10^{-5} M; λ_{ex} = 280 nm, pH = 7.4, T = 298 K.

For static quenching, the bonding constant and the number of binding sites can be obtained by the double logarithm regression curve, which is helpful in the study of pharmacokinetics[50, 51] and is calculated as follows:

$$\log\left(\frac{F_0 - F}{F}\right) = \log K_b + n\log[Q] \quad (4)$$

where K_b is the binding constant and n is the number of binding sites per HSA. Log [(F_0-F)/F] was plotted against log [Q], as shown in Fig. 7. The values of K_b and n were calculated from the values of the intercept and slope of the plots, respectively. All results are listed in Table 2. The binding constants and the number of binding sites increase with increasing temperature, which indicates that temperature affects the binding between SOF and HSA. Compared with other strong drug–protein complexes with binding constants over 10^6 M^{-1}, SOF–HSA has more moderate binding constants. However, low binding constants ranging from 10^3 M^{-1} to 10^4 M^{-1} were still reported for several drug–protein complexes using the fluorescence technique,[18, 22, 26] because drug–protein complexes could result in a high concentration of free drug in plasma. The moderate affinity between SOF and HSA is helpful in the diffusion of SOF from the circulatory system to infected liver cells, which is attributed to a high concentration of free drug in plasma. Our results are consistent with those of the investigations of Li et al.,[26] who have demonstrated that antiviral drugs exhibit weak binding with HSA. In addition, the number of binding sites n approached 1 at three different temperatures, which indicated the presence of one independent binding site on HSA for SOF.

3.3.2 Binding site

Sudlow et al.[23, 24] have demonstrated that HSA has two main binding sites in the hydrophobic pocket, called site I and site II, the markers of which are warfarin and ibuprofen, respectively. To further identify the SOF binding site on HSA, site-marker competition experiments were performed by fluorescence spectroscopy. In our experiments, a solution with fixed amounts of SOF and HSA was titrated by successively adding warfarin or ibuprofen. The experiment results are shown in Fig. 8.

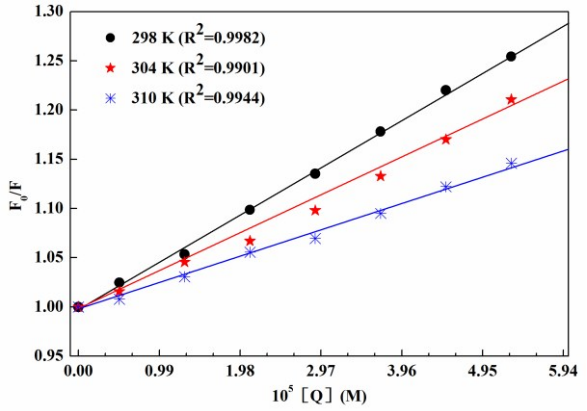

Fig. 6 Stern–Volmer plot of the SOF–HSA system at three different temperatures, C_{HSA}= 2.0×10^{-6} M, C_{SOF}= 0.0–5.3×10^{-5} M, pH = 7.4.

According to the method of Sudlow et al.[24]: $F_1/F_2\times100\%$, where F_1 and F_2 are the fluorescence intensities of SOF–HSA without and with a marker, respectively. The results indicate that warfarin has a greater influence than ibuprofen on the fluorescence intensities of SOF–HSA, which indicates that SOF and warfarin have the same binding site in HSA. Therefore, SOF is most likely bound to site I of HSA, and the finding is consistent with the above NMR finding and docking prediction.

3.3.3 Thermodynamic parameters and binding mode

In general, the noncovalent interaction forces between drugs and biomolecules exist in four types, namely, hydrophobic forces, electrostatic interactions, hydrogen bonds, and van der Waals forces.[18, 19, 36, 47] The binding mode of drugs to proteins can be studied through thermodynamic parameters, such as free energy change (ΔG^0), enthalpy change (ΔH^0), and entropy change (ΔS^0). The thermodynamic parameters ΔH^0 and ΔS^0 can be evaluated according to the following Van't Hoff equation:

$$\ln K_b = -\frac{\Delta H^0}{RT} + \frac{\Delta S^0}{R} \quad (5)$$

where K_b is the binding constant at a corresponding temperature, which can be obtained from fluorescence data, and R is the gas constant. The enthalpy change (ΔH^0) and entropy change (ΔS^0) were obtained from the slope and the intercept of the Van't Hoff plot, respectively. If the variation in temperature range is insignificant, then the enthalpy change ΔH^0 of a system can be considered a constant. The free energy change (ΔG^0) at different temperatures can then be calculated using the following relationship:

$$\Delta G^0 = -RT\ln K_b \quad (6)$$

$$\Delta G^0 = \Delta H^0 - T\Delta S^0 \quad (7)$$

The values of ΔH^0, ΔS^0, and ΔG^0 are listed in Table 2. Ross and Subramanian[52] explained that the signs and magnitude of thermodynamic parameters associated with protein–drug interaction could be employed to evaluate the main forces in protein association processes. The negative ΔG^0 values shown in Table 2 indicated that the binding interaction was

spontaneous; that is, the interaction was an entropically driven process because $T\Delta S^0$ had a larger value than ΔH^0. The ΔH^0 and ΔS^0 values were positive for the SOF–HSA system, which demonstrated that the hydrophobic force played a major role in the binding of SOF to HSA. The experimental free binding energy (−6.18 kcal mol^{-1}) was close to the docking calculated free energy (−7.17 kcal mol^{-1}), which was further verified the feasibility and rationality of the molecular docking method.

3.4 Insights into HSA conformational changes

3.4.1 3.4.1 Synchronous fluorescence spectroscopy

Introduced by Lloyd and Evett[53] in 1977, synchronous fluorescence spectroscopy is helpful in explaining protein microenvironment changes within the vicinity of a chromophore (such as Trp and Tyr residues). This technique involves the simultaneous scanning of the excitation and emission monochromators while maintaining a constant wavelength interval (Δλ) between them. The red or blue shift in the maximum emission reflects the changes in polarity and hydrophobicity around the chromophore molecule. Miller[54] proposed a long-held theory that when Δλ was stabilized at 15 nm and 60 nm, the synchronous fluorescence of HSA would exhibit the characteristic information of Tyr and Trp residues, respectively. The results of the synchronous fluorescence spectra of HSA in the presence of varying SOF concentrations are illustrated in Fig. 9 (a) and (b). As shown in Fig. 9, the maximum emission wavelength presents a faint red shift (from 279 nm to 285 nm) because the concentration of the drug increases gradually when Δλ is stabilized at 60 nm. However, increasing drug concentration is accompanied by a slight decrease in the fluorescence intensity of HSA without imposing any peak position shift at the maximum emission wavelength when Δλ is stabilized at 15 nm. This finding indicates that the binding interaction with SOF leads to an increase in the polarity (decrease in the hydrophobicity) of the microenvironments around the Trp residue.

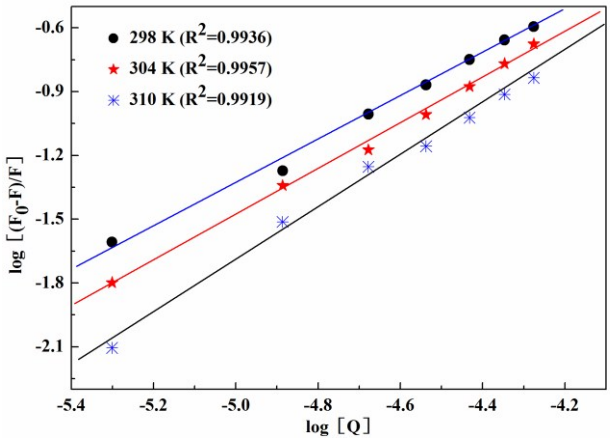

Fig. 7 Plot of log [(F_0−F)/F] vs. log [Q] for the SOF–HSA system at three different temperatures, C_{HSA}= 2.0×10^{-6} M, C_{SOF}= 0.0–5.3×10^{-5} M, pH = 7.4.

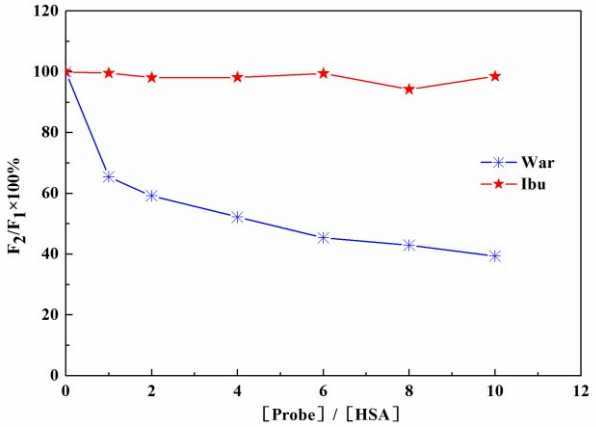

Fig. 8 Effect of warfarin and ibuprofen on the fluorescence of the SOF–HSA system (C_{SOF}= 1.0×10^{-5} M, C_{HSA}= 2.0×10^{-6} M), λ_{ex} = 280 nm, pH = 7.4, T = 298 K.

3.4.2 3D fluorescence spectroscopy.

3D fluorescence spectroscopy is widely used to explore the conformational changes in proteins interacting with drugs.[55] Fig. 10 clearly showed that there were four peaks in the 3D fluorescence spectra for HSA (a) and SOF–HSA systems (b). Peak A and B are the first–ordered Rayleigh scattering peak (λ_{em} = λ_{ex}) and second-ordered scattering peak (λ_{em} = 2λ_{ex}), respectively.[55] Meanwhile, the strong peak 1 mainly reveals the spectral characteristic of Tyr and Trp residues and peak 2 may mainly relates to the fluorescence characteristic of polypeptide backbone structures.[55, 56] Gorinstein et al[56] have demonstrated that the intensity and shift of the peak 2 was correlated with the secondary structures of protein. The corresponding characteristic parameters are shown in Table 3. It can be seen that the fluorescence intensity of peak A increased with the addition of SOF. A large number of studies showed that this phenomenon may be due to the increase of diameter of HSA caused by binding with SOF, which could enhance the Rayleigh scattering peak.[57, 58] The fluorescence intensity of peak 1 decreased at 15.9% after the addition of SOF, which means that the binding of SOF with HSA changed the micro-environmental of Tyr and Trp residues. The result was in accordance with that obtained from the foregoing synchronous fluorescence results. Besides, the intensity of peak 2 has also been decreased about 15.7%, which indicated that the polypeptide backbone structures of protein changed. All the differences in the 3D fluorescence intensity suggested a specific sort of interaction between SOF and HSA resulted in some micro-environmental and conformational changes in HSA.

3.4.3 FT-IR spectroscopy

To further investigate the conformational change of HSA, FT-IR measurements were performed in the absence and presence of SOF. The differences in FT-IR spectra of a protein can demonstrate different amide bands vibration of the peptide moieties. Most investigations have been reported that the amide I and amide II peak are in the region of 1700–1600 cm^{-1} (mainly attributable to C=O stretching) and 1600–1500 cm^{-1} (C–N stretch coupled with N–H bending mode),

respectively,which are sensitive to the secondary structure of proteins.[55, 59] As shown in Fig.9 (c), the FT-IR spectra of HSA and SOF–HSA were obtained by subtracting absorption spectra of PBS and SOF solution, respectively. It is observed that the characteristic amide I and II absorption peak positions of free HSA were at 1650.77 and 1550.49 cm^{-1}, respectively. Whereas the peak position of amide I and II clearly shifted to 1646.91 cm^{-1} and 1546.63 cm^{-1} after binding with SOF,respectively. Dong et al[60] have proved that the spectral range from 1662 to 1650 cm^{-1} attributed to α-helices in the amide I bands as early as 1990. Therefore, the peak position shift of amide I along with the decrease in peak intensity, implying the α-helical content of HSA has been changed due to the binding with SOF. All these changes in the peak positions and intensities demonstrated that the SOF entered into the hydrophobic cavity of HSA and interacted with the C=O and C-N groups in the protein polypeptides, leading to conformational changes in the secondary structure of HSA.[55, 59]

3.4.4 CD spectroscopy

CD spectroscopy is another effective approach to monitor the secondary structural changes of a protein upon interaction with drugs. In Fig. 9 (d), the CD spectrum of free HSA presented two negative absorption bands at 208 nm and 222 nm in the ultraviolet region, which are characteristics of a typical α-helical structure of protein.[22, 59] The α-helical content of HSA can be calculated from mean residue ellipticity (MRE) at 208 nm using Equation (6), as follows:[18, 19, 36]

$$\alpha\text{-helix}\ (\%) = \frac{-MRE_{208} - 4000}{33000 - 4000} \times 100 \qquad (8)$$

where 4000 and 33000 are the MRE values of a β-form with random coil conformation and a pure α-helix at 208 nm, respectively. MRE_{208} is the observed CD value at 208 nm, which is transformed according to the following equation:[18, 19, 36]

$$\mathrm{MRE} = \frac{ObseredCD(m\deg)}{10 \times C_p nl} \qquad (9)$$

where C_p is the molar concentration of the protein, n is the number of amino acid residues (585), and l is the path length (0.2 cm).

As shown in Fig. 9 (d), adding SOF does not generate obvious shifts in the position of 208 nm and 222 nm, which suggests that the structure of HSA was also predominantly α-helix. Using the preceding equations, the α-helical contents were calculated to be 57.8% (free HSA), 57.2%, and 55.5% at a molar ratio of SOF to HSA of 0, 5, and 15, respectively. A slight decrease in the α-helical content of HSA indicates that adding SOF induces a partial unfolding of the secondary structure of HSA. Gokara et al.[61] deemed that the partial unfolding could be attributed to micro-environment changes around chromophores while binding to HSA, which was consistent with the results of synchronous and 3D fluorescence, and FT-IR spectroscopy.

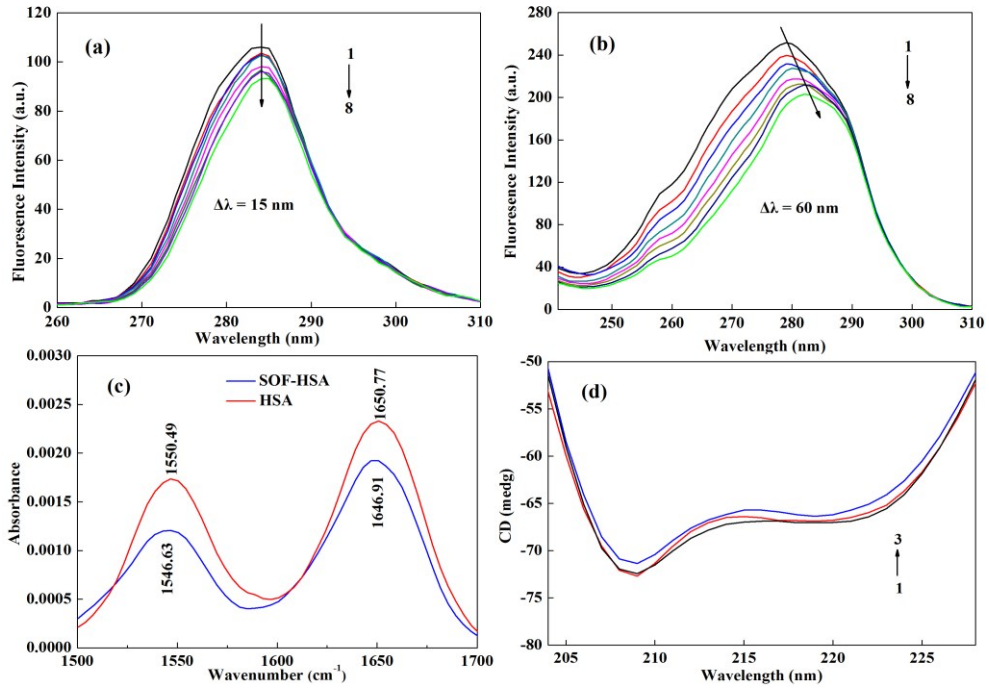

Fig. 9 Effect of SOF on the HSA conformation. Synchronous fluorescence spectra of HSA in the presence of varying concentrations of SOF for Δλ = 15 nm (a) and Δλ = 60 nm (b), Curves 1 → 8 correspond to C_{SOF} = 0, 0.5, 1.3, 2.1, 2.3, 3.7, 4.5, 5.3×10^{-5} M; FT-IR spectra (C), $C_{HSA} = 2\times10^{-4}$ M, $C_{SOF} = 1\times10^{-3}$ M; CD spectra of HSA in the absence and presence of SOF (d). $C_{HSA} = 3\times10^{-6}$ M. Curves 1 → 3 correspond to the molar ratio of SOF to HSA of 0, 5, and 15.

Table 2 Binding and thermodynamic parameters of the SOF–HSA system.

T (K)	K_{sv} ($\times10^3$ M^{-1})	κ_q ($\times10^{11}$ M^{-1} s^{-1})	n	K_b ($\times10^3$ M^{-1})	ΔH^0 (kcal mol^{-1})	ΔG^0 (kcal mol^{-1})	$T\Delta S^0$ (kcal mol^{-1})
298	4.87±0.08	4.87±0.08	1.01±0.03	5.43±0.01		-5.09±0.21	27.46±3.26
304	3.91±0.15	3.91±0.15	1.08±0.03	8.04±0.01	22.36±6.30	-5.41±0.19	27.78±3.24
310	2.77±0.08	2.77±0.08	1.21±0.05	23.65±0.02		-6.18±0.29	28.55±3.30

Table 3 3D fluorescence spectral parameters of HSA alone and in the presence of SOF

	HSA			SOF–HSA		
	Peak position		stokes	Peak position		stokes
peak	λex / λem (nm/nm)	Δλ (nm)	Intensity F	λex / λem (nm/nm)	Δλ (nm)	Intensity F
A	280/280→350/350	0	332.24→568.74	280/280→350/350	0	77.94→635.73
1	280/340	60	815.76	280/340	60	685.92
2	225/331	106	729.27	225/334	109	614.70

4. Conclusions

The binding mechanism of SOF with HSA was investigated using the ^{1}H STD–NMR and WaterLOGSY–NMR technique, the molecular docking method, and different optical spectroscopy techniques under simulated physiological conditions. The ^{1}H NMR technique and the molecular docking study provided a theoretical direction to obtain reliable experimental results, which clearly demonstrated that the SOF molecule could be inserted into the hydrophobic cavity of HSA. In particular, the hydrophobic portion of SOF was the most tightly bound to HSA. Additional steps in the fluorescence studies revealed that HSA fluorescence could be statically quenched by SOF at a single binding site (i.e., site I). Synchronous and 3D fluorescence, FT-IR spectroscopy, CD measurements showed that the binding of SOF to HSA induced the changes in the micro-environments of the protein and decreased the α-helical contents. Overall, this study is helpful to improve understanding of the interaction between antiviral drugs and HSA as well as to facilitate further investigations on the pharmacokinetic and pharmacodynamic behavior of antiviral drugs.

Acknowledgements

This work was supported by the Applied Basic Research Project of Sichuan province (Grant No. 2014JY0042) and the Testing Platform Construction of Technology Achievement Transform of Sichuan Province (Grant No. 13CGPT0049). The authors would like to thank the professors of Analytical & Testing Center Sichuan University, P. R. China for their generous advice and assistance on the NMR experiments. We would also like to thank the editors of Enpapers for editing the manuscript.

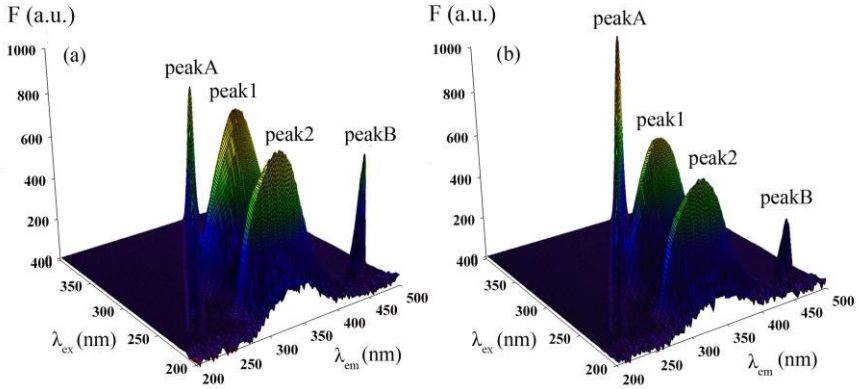

Fig. 10 3D fluorescence spectra of (a) HSA and (b) SOF–HSA system. C_{SOF}= 2.0×10^{-5} M, C_{HSA}= 2.0×10^{-6} M; λ_{ex} = 200–400 nm, λ_{em} = 200–500 nm.

References

1 Y. Waheed, *World J Virol.*, 2015, **4**, 33-35.
2 L. Y. Lee, C. Tong, T. Wong and M. Wilkinson, *Int. J. Clin. Pract.*, 2012, **66**, 342-355.
3 M. J. Sofia, D. Bao, W. Chang, J. Du, D. Nagarathnam, S. Rachakonda, P. G. Reddy, B. S. Ross, P. Wang, H. R. Zhang, S. Bansal, C. Espiritu, M. Keilman, A. M. Lam, H. M. Steuer, C. Niu, M. J. Otto and P. A. Furman, *J. Med. Chem.*, 2010, **53**, 7202-7218.
4 Z. M. Younossi, H. Park, S. Saab, A. Ahmed, D. Dieterich and S. C. Gordon, *Aliment. Pharmacol. Ther.*, 2015, **41**, 544-563.
5 H. Leleu, M. Blachier and I. Rosa, *J. viral hepatitis*, 2015, **22**, 376-383.
6 A. J. van der Meer, B. J. Veldt, J. J. Feld, H. Wedemeyer, J.-F. Dufour, F. Lammert, A. Duarte-Rojo, E. J. Heathcote, M. P. Manns and L. Kuske, *Jama*, 2012, **308**, 2584-2593.
7 E. Lawitz, J. P. Lalezari, T. Hassanein, K. V. Kowdley, F. F. Poordad, A. M. Sheikh, N. H. Afdhal, D. E. Bernstein, E. DeJesus, B. Freilich, D. R. Nelson, D. T. Dieterich, I. M. Jacobson, D. Jensen, G. A. Abrams, J. M. Darling, M. Rodriguez-Torres, K. R. Reddy, M. S. Sulkowski, N. H. Bzowej, R. H. Hyland, H. Mo, M. Lin, M. Mader, R. Hindes, E. Albanis, W. T. Symonds, M. M. Berrey and A. Muir, *Lancet Infect. Dis.*, 2013, **13**, 401-408.
8 N. Fujita, M. Nakanishi, J. Mukai, Y. Naito, T. Ichida, M. Kaito, T. Yoshikawa and Y. Takei, *Mol. Med.*, 2011, **17**, 70-78.
9 G. M. Abraham and L. M. Spooner, *Cli. Infect. Dis.*, 2014, **59**, 411-415.
10 W. Shenfeng, L. Jianping, H. Peilan, Z. Jianping and L. Yaqiu, *Acta Chim. Sinica*, 2014, **72**, 906-913.
11 M. S. Sulkowski, D. F. Gardiner, M. Rodriguez-Torres, K. R. Reddy, T. Hassanein, I. Jacobson, E. Lawitz, A. S. Lok, F. Hinestrosa and P. J. Thuluvath, *New Engl. J. Med.*, 2014, **370**, 211-221.
12 T. C. Appleby, J. K. Perry, E. Murakami, O. Barauskas, J. Feng, A. Cho, D. Fox, D. R. Wetmore, M. E. McGrath and A. S. Ray, *Science*, 2015, **347**, 771-775.
13 M. P. Manns and M. Cornberg, *Lancet Infect. Dis.*, 2013, **13**, 378-379.
14 E. Lawitz, A. Mangia, D. Wyles, M. Rodriguez-Torres, T. Hassanein, S. C. Gordon, M. Schultz, M. N. Davis, Z. Kayali and K. R. Reddy, *New Engl. J. Med.*, 2013, **368**, 1878-1887.
15 Q. Wang, X. L. Ma, J. W. He, Y. Z. Li and H. Li, *RSC Adv.*, 2015, **5**, 44696-44704.
16 Y. J. Hu, Y. Liu, X. S. Shen, X. Y. Fang and S. S. Qu, *J. Mol. Struct.*, 2005, **738**, 143-147.
17 X. Q. Wu, W. J. Zhu, Z. R. Lu, Y. Xia, J. M. Yang, F. Zou and X. Y. Wang, *Int. J. Biol. Macromol.*, 2009, **44**, 149-155.
18 N. Shahabadi, S. Hadidi and F. Feizi, *Spectrochim. Acta, Part A.*, 2015, **138**, 169-175.
19 N. V. Rakotoarivelo, P. Perio, E. Najahi and F. Nepveu, *J. Phys. Chem. B.*, 2014, **118**, 13477-13485.
20 D. Wu, Y. Zhai, J. Yan, K. Xu, Q. Wang, Y. Li and H. Li, *RSC Adv.*, 2015, **5**, 11036-11042.
21 P. C. A. G. Pinto, D. M. G. P. Ribeiro, A. M. O. Azevedo, V. Dela Justina, E. Cunha, K. Bica, M. Vasiloiu, S. Reis and M. L. M. F. S. Saraiva, *New J. Chem.*, 2013, **37**, 4095.
22 X. Li and S. Wang, *New J. Chem.*, 2015, **39**, 386-395.
23 G. Sudlow, D. J. Birkett and D. N. Wade, *Mol. Pharmacol.*, 1975, **11**, 824-832.
24 G. Sudlow, D. J. Birkett and D. N. Wade, *Mol. Pharmacol.*, 1976, **12**, 1052-1061.
25 M. Ishtikhar, G. Rabbani and R. H. Khan, *Colloids Surf. B, Biointerfaces*, 2014, **123**, 469-477.
26 M. Li, E. McAuley, Y. Zhang, L. Kong, F. Yang, Z. Zhou, X. Wu and H. Liang, *Chem. Biol. Drug Des.*, 2014, **83**, 576-582.
27 N. Shahabadi, Z. M. Kalar and A. V. Rayegani, *DNA and cell Bio.*, 2012, **31**, 876-882.
28 L. Hagan, Z. Yang, M. Ehteshami and R. Schinazi, *J. viral hepatitis*, 2013, **20**, 847-857.
29 C. Rafols, S. Zarza and E. Bosch, *Talanta*, 2014, **130**, 241-250.
30 M. H. Rahman, T. Maruyama, T. Okada, T. Imai and M. Otagiri, *Biochem. Pharmacol.*, 1993, **46**, 1733-1740.
31 L. Trnková, I. Boušová, V. Staňková and J. Držata, *J. Mol. Struct.*, 2011, **985**, 243-250.
32 J. Yan, Y. L. Cai, Y. Wang, X. Lin and H. Li, *Food Chem.*, 2014, **143**, 82-89.
33 B. K. Paul and N. Guchhait, *Photoch. Photobio. Sci.*, 2011, **10**, 980.
34 J. Yan, Q. Wang, Q. Q. Pan, Z. Sh. Rao, Y. H. Su and H. Li, *J. Lumin.*, 2013, **137**, 180-185.
35 M. Mayer and B. Meyer, *J. Am. Chem. Soc.*, 2001, **123**, 6108-6117.
36 X. Zhou, X. Li and X. Chen, *Dyes and Pigments*, 2013, **98**, 212-220.
37 J. Pérez-Castells, M. Fontanella, A. Ardá, F. J. Canãda, M. Sollogoub, Y. Blériot and J. Jiménez-Barbero, *New J. Chem.*, 2012, **36**, 1008.
38 Y. S. Wang, D. Liu and D. F. Wyss, *Magn. Reson. Chem.*, 2004, **42**, 485-489.
39 D. M. Dias, J. P. Rodrigues, N. S. Domingues, A. M. Bonvin and M. Castro, *Eur. J. Inorg. Chem.*, 2013, **2013**, 4619-4627.
40 A. Sivertsen, J. Isaksson, H. K. S. Leiros, J. Svenson, J.-S. Svendsen and B. O. Brandsdal, *BMC Struct. Biol.*, 2014, **14**, 4.
41 D. Gossert, C. Henry, M. J. Blommers, W. Jahnke and C. Fernández, *J. Biomol. NMR*, 2009, **43**, 211-217.
42 B. K. Paul and N. Guchhait, *J. Phys. Chem. B.*, 2011, **115**, 10322-10334.
43 B. K. Paul, D. Ray and N. Guchhait, *Phys. Chem. Chem Phys.*, 2013, **15**, 1275-1287.
44 E. Aghaee, J. Ghasemi, F. Manouchehri and S. Balalaie, *J. Mol. Model*, 2014, **20**, 1-13.
45 K. Zheng, F. Liu, X. M. Xu, Y. T. Li, Z. Y. Wu and C. W. Yan, *New J. Chem.*, 2014, **38**, 2964-2978.
46 A. S. Sharma, S. Anandakumar and M. Ilanchelian, *RSC Adv.*, 2014, **4**, 36267.
47 X. Li, G. Wang, D. Chen and Y. Lu, *Food Chem.*, 2015, **179**, 213-221.
48 J. R. Lakowicz, B. R. Masters, *J. Biomed. Opt.*, 2008, **13 (2)**, 029901-029902.
49 W. R. Ware, *J. Phys. Chem.*, 1962, **66 (3)**, 455-458.
50 X. Z. Feng, Z. Lin, L. J. Yang, C. Wang and C. L. Bai, *Talanta*, 1998, **47**, 1223-1229.
51 E. Lissi, C. Calderón and A. Campos, *Photochem. Photobiol.*, 2013, **89**, 1413-1416.
52 P. D. Ross and S. Subramanian, *Biochemistry*, 1981, **20**, 3096-3102.
53 J. Lloyd and I. Evett, *Anal.l Chem.*, 1977, **49**, 1710-1715.
54 J. N. Miller, *The Analyst*, 1984, **109**, 191-198.
55 H. X. Zhang, X. Huang, P. Mei, K. H. Li and C. N. Yan, *J. Fluoresc.*, 2006, **16**, 287-294.
56 S. Gorinstein, I. Goshev, S. Moncheva, M. Zemser, M. Weisz, A. Caspi, I. Libman, H. T. Lerner, S. Trakhtenberg and O. Martín-Belloso, *J. protein chem.*, 2000, **19**, 637-642.
57 P. Zhang, Z. Li, X. Wang, Z. Shen, Y. Wang, J. Yan, Z. Zhou and W. Zhu, *Chirality*, 2013, **25**, 719-725.
58 Q. Wang, J. He, D. Wu, J. Wang, J. Yan and H. Li, *J. Lumin.*, 2015, **164**, 81-85.
59 X. Peng, X. Wang, W. Qi, R. Su and Z. He, *Food Chem.*, 2016, **192**, 178-187.

60 A. Dong, P. Huang and W. S. Caughey, *Biochemistry*, 1990, **29**, 3303-3308.
61 M. Gokara, T. Malavath, S. K. Kalangi, P. Reddana and R. Subramanyam, *J. Biomol. Struct. Dyn.*, 2014, **32**, 1290-1302.

The qualitative and quantitative investigation of sofosbuvir and HSA interaction provides a convictive explanation for its binding mechanism.

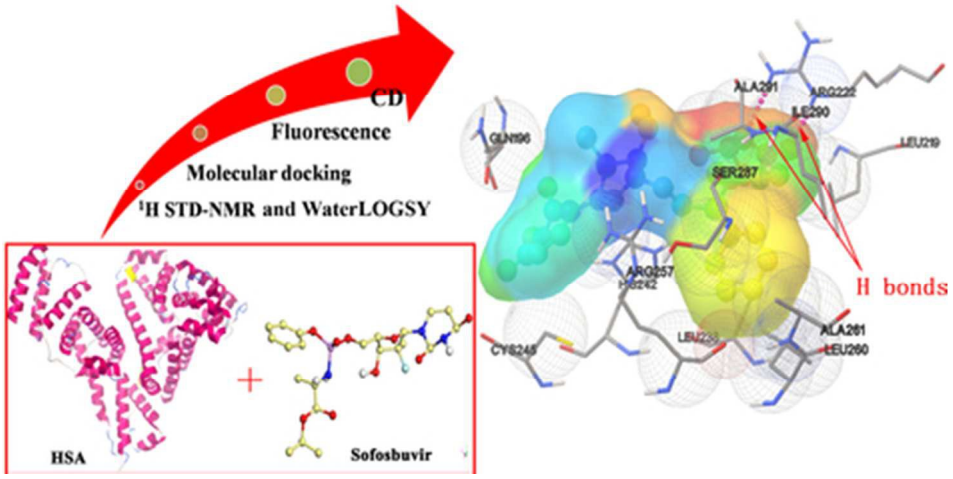

39x19mm (300 x 300 DPI)